LFC for Autonomous Hybrid Micro Grid System of 3 Unequal Renewable Areas using Mine Blast Algorithm

Sudhanshu Ranjan*‡, D C Das*, A. Latif*, N Sinha*

*Department of Electrical Engineering, National Institute of Technology Silchar, 788010, Assam, India

(ranjan4c@gmail.com, dulal_nit@yahoo.co.in, latif1014@gmail.com, nidulsinha@hotmail.com)

‡ Sudhanshu Ranjan: National Institute of Technology Silchar, 788010, Assam, India, Tel: +91 8638150629, ranjan4c@gmail.com

Received: 26.03.2018 Accepted:08.05.2018

Abstract: This paper ensures the feasibility of the proposed 3-area hybrid micro grid system (3A-HμGS) comprising of highly intermittent energy sources like wind turbine generator (WTG), parabolic trough collector (PTC), and PV arrays. Renewable energy sources (RES) inherently set in power and frequency oscillations as these sources (RES) are extremely influenced by climatic behavior that's why the erection of 3A-HμGS as a controlled dispatchable unit is in fact very difficult to be realized. This proposed system has considered diesel engine generator (DEG) as a back-up source and the energy storage system (ESS) like battery, ultra-capacitor and fuel cell as the dynamic devices to make it controllable and reliable. Unwanted frequency deviation has been restricted to a satisfactory limit through GA, PSO and MBA based proportional integral derivative (PID), proportional integral derivative with filter (PIDN) and 2 degree of freedom PID (2DOF-PID) controllers. MBA based 2DOF-PID controllers provide the best coordination among RES, ESS, and DEG to maintain the power quality of 3A-HμGS. A qualitative and quantitative analysis of the dynamic responses under all the controlling actions clearly exhibits the efficacy of the proposed system. Moreover, the system remains stable even after incorporation of natural disturbances like change in wind velocity and solar irradiances which ensure the feasibility and practicality of the proposed 3A-HμGS.

Key words*:* Load frequency control (LFC); parabolic trough collector (PTC); 3-area hybrid micro grid system (3A-HμGS); mine blast algorithm (MBA);

Nomenclatures:

R_1, R_2 *and* R_3	Droops in area-1, area-2 and area-3 respectively
B_1, B_2 and B_3	Frequency biasing
T_{12}, T_{13}, *and* T_{23}	Synchronizing coefficients
ΔF_1, ΔF_2, and F_3	Frequency deviations in area-1, area-2 and area-3 respectively
$\Delta P_{tie\ 1.2}$, $P_{tie\ 1.3}$, and $\Delta P_{tie\ 2,3}$	Deviations in the power exchange of the tie lines
P_{WT}	Power of wind turbine
C_P	Performance coefficient
B	Pitch angle
Λ	Tip speed ratio
P	Air density (1.2 to 1.25 kg/m3)
η_{MPPT}	Efficiency of MPPT
A	Area swept by the blades
v_W	Wind velocity
$c_1 - c_8$	Constants
w_t	Turbine mechanical speed
r	Radius of swept area
v_{cut-in}, $v_{cut-out}$	Cut-in wind speed, maximum cut-out Wind speed
v_{rated}	Nominal wind speed
Δv_W	Deviation in wind velocity
$P_{solar}, \Delta P_{solar}$	Solar output power and its deviation
P_{PV}	Rated power at standard test condition (STC)
G	Solar radiation for PV arrays in W/m^2
G_{STC}	Reference sun irradiance for PV arrays at STC 1000(W/m^2)
T_{STC}	Reference temperature (i.e. 25°C)
K_t	Constant −0.0037 °C−1
T_a	Ambient temperature.

ΔG, and ΔT_a	Deviation in irradiance and temperature respectively
T_{WTG}, T_{PTC}, T_{PV}, T_{DEG}, $T_{BESS}, T_{UC}, and\ T_S$	Time constant of wind turbine generator, parabolic trough solar power, PV arrays, diesel generator, BESS, UC, and SMES respectively
$K_{WTG}, K_{PTC}, K_{PV,}$ $K_{DEG}, K_{BESS}, K_{UC},$ $and\ K_{SMES}$	Gain of WTG, PTC, PV arrays, DEG, BESS, UC, and SMES respectively
$T_{P1}, T_{P2}, and\ T_{P3}$	Rotor oscillating time constants
$K_{P1}, K_{P2}, and\ K_{P3}$	Gain of the rotor swing of area-1, area-2, and area-3 respectively

1. Introduction

In last few decades, the whole world has got a great concern over climatic change and its unavoidable consequences which might put all mankind in danger. A perspective towards saving climate to save the world has made us think of renewable power generation at best. This intensive concern leads all the researchers and the companies in making the most of abundant, clean, and non-polluting resources like solar thermal, wind, and PV arrays etc.

Out of all renewable sources, solar thermal power is highly encouraging and being installed widely. Parabolic trough solar thermal system is one of the developed and proven solar thermal technologies with significant potential to contribute in energy sector [1]. Spain leads the way with installed capacity of 2370 MW, followed by USA of 1,836 MW. In Spain, each plant (50 MW) provides electricity up to 2 million people and reduces around 149 thousand tons of CO2 per year compared to coal based power generation whereas in Solana, it provides sufficient amount of electricity to around 71 thousand homes and saves the environment from 42.7 thousand tons of carbon emission each year [2].

Moreover, the integration of two or more than two of them as hybrid energy system or hybridized micro grid system is highly preferable [3], [4].

However, the intermittent nature of RESs create an importance of energy storing elements like battery, aqua electrolyzer (AE), fuel cell (FC), ultra capacitor, super magnetic energy storage (SMES), and many more [6-9]. This intermittent nature causes power and frequency oscillation [7, 8] and sometimes result in unstable operation of the system. Having controlled the energy storage system, supply through renewable sources on large scale can be controlled to some extent and used as a dispatch able unit on small scale [10].

Having concerned with the nature's unpredictable characteristics and customers' power requirement at constant voltage and constant frequency, reliable and stable hybrid system includes DEGs as a back-up source of supply for immediate load demand. The ESSs are somewhat capable of leveling the power fluctuations but unable to alter the generation to meet the power demand. Maintaining power balance condition is utmost important for stable operation of the micro grid. Automatic load frequency control is used for the same. Many papers [11-15] have made their analysis on LFC for hybrid power system using different artificial intelligence-based methods such as genetic algorithm (GA), particle swarm optimization (PSO), fuzzy logic control and so on. Flower Pollination Algorithm (FPA), and Firefly Algorithm (FA) have been used in [29] and [31] to contain the frequency of isolated hybrid power system. Bacteria Foraging Optimization Algorithm (BFOA), Differential Evolution (DE), and Teaching Learning Based Optimization [16] have been used in AGC. Recently, Social spider optimizer (SSO) [5] has been used to optimize PID controllers in containing frequency of two area hybrid microgrid. In this work, two isolated hybrid areas are interconnected with renewable energy like, wind energy in one area and solar PV the other. System performance has been satisfactory under different generating and loading scenarios. However, frequency control strategy of hybrid microgrid in presence of some other renewable energy technology using different controller remains unexplored.

In view of the above this work focuses on frequency control of three area hybrid micro grid system. All the three areas consist of only renewable energy sources like wind, parabolic trough collector, and PV arrays integrated with diesel engine generators. To overcome the uncertainties of the sources and to improve the dynamic performance of the proposed model, all three areas are equipped with SMES, UC, and BESS respectively. To show the practicality of the SIMULINK model, realistic features like wind speed variation and change in solar irradiance are incorporated.

This paper addresses the following objectives:

1. Development of SIMULINK/transfer function model of 3A-HμGS for its dynamic behavior and practical significance.
2. Integration of PTC as a source in a 3A-HμGS for the first time and obtaining proper coordination between ESSs and RESs.

3. Maiden application of PIDN, and 2DOF-PID controllers for such a 3A-HµGS with their gains optimized through GA, PSO, and MBA for frequency control.
4. Examine the performance of the controllers in 3A-HµGS considering degree of robustness and controllability under different generating and loading condition.

2. Configuration and Mathematical Modeling of 3A-HµGS

A complete Laplace transfer function model of 3A-HµGS has been realized in this work and shown in Figure. 1(b). WTGs, Parabolic Troughs, and PVs are the power generating sources to fulfill the required demand. Since these sources are having a great degree of randomness, diesel generators are taken into consideration as a complementary source of power generation to ensure the system reliability. A proposed HµGS becomes very much reliable because DEG stands as the back-up source to reduce the gap in between generation and load demand of the system.

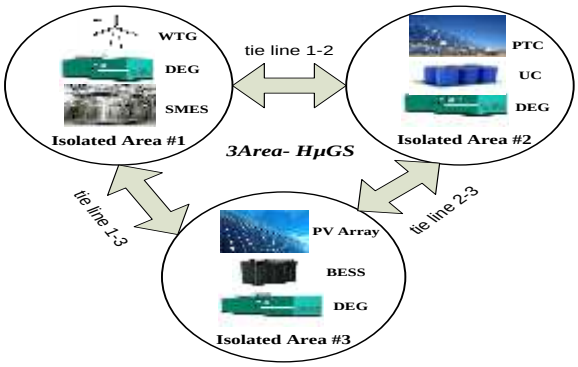

(a)

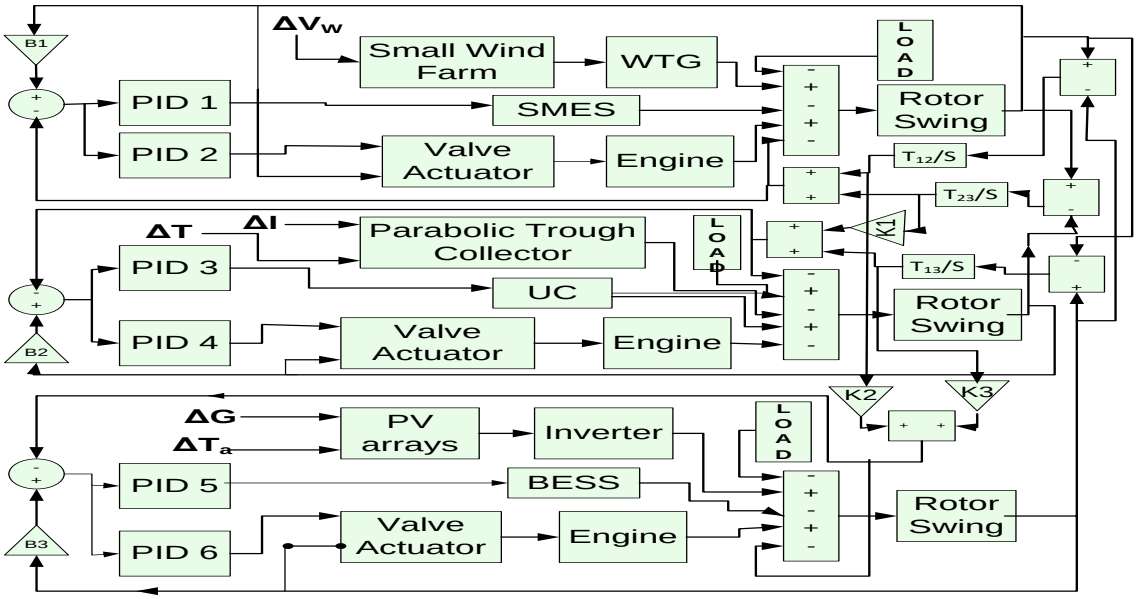

(b)

Fig.1. (a) Schematic diagram and (b) block diagram of the proposed 3A- HµGS

Here ESSs are used to control frequency deviation efficiently under change in load. These ESSs store energy when the generation through RESs exceeds the system load demand and delivers energy back to the system during peak time. PID controllers are incorporated with DEGs and ESSs to damp out the oscillations and to maintain the frequency and tie line powers within reasonable values. The characteristics of different components of 3A-HµGS have been described briefly which are as follows:

2.1. Modeling of Wind Turbine Generator (WTG)

Output power of WTG can be expressed as [17]

$$P_{WT} = 0.5\, C_P(\beta,\lambda).\rho\, A\, v_w^2 \quad (1)$$

The performance coefficient C_P [17] is calculated using the following equations.

$$C_P(\beta,\lambda) = C_1(C_2/\lambda_r - \beta C_3 - C_4)e^{(-C_5/\lambda_r)} + C_6\lambda_r \quad (2)$$

$$\frac{1}{\lambda_r} = 1/(\lambda + \beta C_7) - C_8/(1+\beta^3)\ and\ \lambda = \frac{rW_t}{v_W} \quad (3)$$

For the optimum operation of wind turbine, C_P is mostly controlled in between low and medium wind velocity. In this study, GAMESA power wind turbine [18] has been considered where 5 WTGs have been connected together whose overall rated capacity is 4250 kW [18]. Output power of

the WTG can be computed through equation (4). However, the change in power output is calculated as shown in eqn. (5).

$$P_{WT} = \begin{cases} 0, & v_{cut-in} > v_w < v_{cut-out} \\ P_{rated}, & v_{rated} \le v_w \le v_{cut-out} \\ 0.001312v_w^6 - 0.4603v_w^5 + 0.3314v_w^4 \\ +3.687v_w^3 - 51.1v_w^2 + 2.33v_w + 366, else \end{cases} \quad (4)$$

$$\Delta P_{WT} = (0.007872v_w^5 - 0.23015v_w^4 + 1.3256v_w^3 + 11.061v_w^2 - 102.2v_w + 2.33)\Delta v_w \quad (5)$$

2.2. Modeling of PV Arrays

Solar output power mainly depends on solar irradiance and temperature. It is having linear relation with G if ambient temperature is fixed at 25^{0}C. Output power of solar can be calculated through equation (6) and change in output power with the change in solar irradiance and temperature is computed through (7) [19, 20]. This study considers five PV arrays connected together each rated with 200 kW at STC and maximum power point tracker (MPPT) with 98% efficiency.

$$P_{solar} = P_{PV}G/G_{STC}[1 + k_t\begin{pmatrix} T_a + 0.0256G \\ -T_{STC} \end{pmatrix}]\,\eta_{MPPT} \quad (6)$$

$$\Delta P_{solar} = P_{PV}/G_{STC}[\Delta G + k_t(T_a\,\Delta G + \Delta T_a + 0.0512G\,\Delta G - T_{STC}\Delta G)]\,\eta_{MPPT} \quad (7)$$

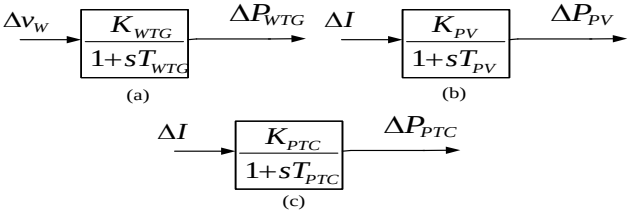

Fig. 2. Transfer function model of WTG, PV arrays, and PTC

2.3. Modeling of Parabolic Trough Collector (PTC)

Output of parabolic trough solar thermal system depends on solar irradiance and fluid temperature. Water, steam, or synthetic oil as heat transfer fluid (HTF) is heated for steam generation at 400^{0}C where steam drives the turbine to generate the electricity. This study considers SEGS LS-2 parabolic trough collector [21] whose efficiency (η_C) is computed through equation (8). Steam generator (η_g) and turbine (η_T) efficiency are assumed at 98% and 37.5% respectively [22]. Overall efficiency (i.e. $\eta_{overall}$ =38%) of parabolic trough solar power plant can be computed as (10). There are four solar collectors connected together make one loop with the rating of 0.5 MW. However, six loops have been considered in this paper with total capacity of 6 MW [23] and efficiency of the collector is given by

$$\eta_C = k[73.8 - 0.006460\,\Delta T] - 12.16\Delta T/I - 0.0641\,(\Delta T)^2/I \quad (8)$$

$$k = \cos\theta - 0.0003512\theta - 0.00003137\theta^2 \quad (9)$$

ΔT is difference between fluid temperature (T_f) and ambient temperature (T_a) in degree Celsius, I is direct normal irradiance equal to 873 W/m^2, and k is incident angle modifier (θ=60^0 assumed in this study). Change in efficiency of collector with respect to direct normal irradiance (I) can be calculated as follows:

$$\Delta\eta_C = \Delta I/I^2(12.16\Delta T + 0.0641(\Delta T)^2 \quad (10)$$

$$P_{PTC} = \eta_{overall}\ \mathrm{X}\ P_{input} \quad (11)$$

Where, $\eta_{overall} = \eta_C\eta_g\eta_T$

Change in power can be written as

$$\Delta P_{PTC} = \Delta\eta_C\eta_g\eta_T \mathrm{X}\ P_{input} \quad (12)$$

Transfer function model of the WTG, PV arrays, and PTC are shown in Figure 2 (a), (b), and (c) respectively.

2.4. Modeling of Diesel Engine Generator

The power availability of wind, solar thermal, and PV arrays entirely depends on wind, temperature and solar patterns respectively hence renewable energy sources are combined with DEGs for continuous power supply.

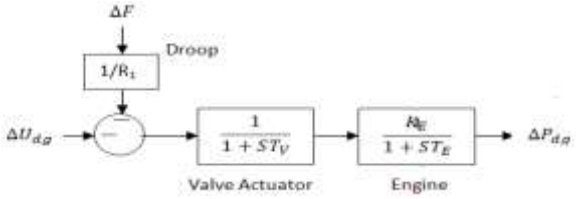

Fig. 3 *Transfer Function of DEG*

Speed governor is coupled with DEGs for speed regulation of the diesel engine [24-27] which has been represented in Figure. 3. A valve actuator with first order time delay (T_V) and droop control loop with droop R have been considered. DEGs taken in this study has rating of 500 kVA for each area. Diesel generator has high dynamic response to the load variations. It has the capability to respond 100% load demand with immediate effect [28]. On the other hand DEGs are always avoided from overloading for satisfactory operation. In this study, overloading can be successfully handled by DEGs with the combination of PEVs.

2.5. Modeling of Battery Energy Storage System (BESS)

BESS is inevitable device for the isolated system especially running on RESs. In BESS, battery bank is interfaced with the isolated system through power converters. BESS has dynamic property to damp out the frequency oscillation by absorbing surplus power and dispatching deficit amount of power as required by the system. The mathematical Laplace transfer function model of BESS can be given by the following equation [29].

$$G_{BESS} = \frac{K_{BESS}}{1+ST_{BESS}} \quad (13)$$

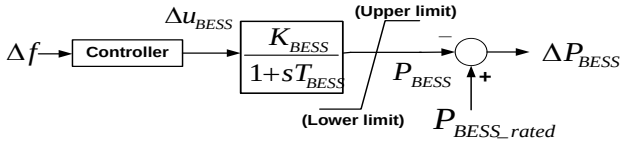

Fig. 4 Transfer function model of BESS

2.6. Modeling of Ultra Capacitor (UC)

A double-layer ultra-capacitor comprises of electrode, electrolyte, collector and diaphragm. Its temperature range during operation is comparatively wider and it has stable operating characteristics. Complexity of chemical reaction is absent during its operation, so it can be realized for higher rate of charging and discharging phenomena. This high speed charging and discharging process of capacitor reduces the difference between load demand and generation resulting in smaller deviation and responses of the system settle down immediately. Transfer function equation of UC is given in equation.

$$G_{UC} = \frac{K_{UC}}{1+ST_{UC}} \quad (14)$$

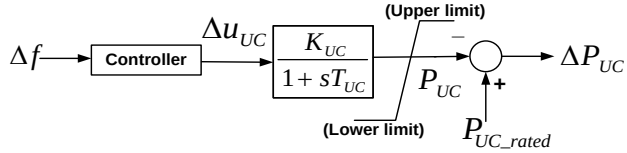

Fig. 5 Transfer function model of UC

2.7. Modeling of SMES

Superconducting magnetic energy storage (SMES) is an energy storage device which stores energy in the form of magnetic field ($0.5LI^2$). Energy is stored cryogenically in the superconducting wire by keeping its temperature below its superconducting critical temp. Its efficiency is greater than 95% during energy storing process which is higher than any other energy storage devices. The transfer function equation of SMES is shown by the following equation.

$$G_{SMES} = \frac{K_{SMES}}{1+ST_{SMES}} \quad (15)$$

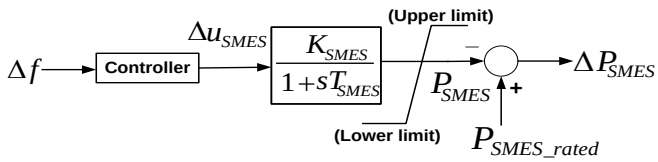

Fig. 6 Transfer function model of SMES

3. Problem Formulation

Parameters of PID controllers are optimally tuned by considering all areas frequency deviations and tie-line powers. Different types of integral criterions are being used to set the objective function. Objective function considered for any problem plays a vital role for the improvement in dynamic responses of the system. Hence to define the objective function (J) for this study, ISE has been considered [30].

$$J = \int_0^{T_S} ((|\Delta F_i|)^2 + (|\Delta P_{tie j-k}|))^2)\, dt$$

$$where\ i = 1\ to\ 3,\ j = 1,2\ and\ k = 2,3 \quad (16)$$

J is minimized subjected to the following constraints.

$$K_p^{\min} \le K_p \le K_p^{\max} \quad (17)$$

$$K_i^{\min} \le K_i \le K_i^{\max} \quad (18)$$

$$K_d^{\min} \le K_d \le K_d^{\max} \quad (19)$$

K_P, K_I, and K_D are the proportional, integral and derivative gain of the PID controllers respectively.

Separate PID, PIDN, and 2DOF-PID controllers are used in the system for all DEGs and ESSs. PID with filter (PIDN) and 2DOF-PID controllers are better than the traditional PID controller. PIDN consists of low pass filter which removes the higher frequency harmonics and settles down the waveform at a very fast rate whereas 2DOF-PID has two more tunable parameters B_i and C_i apart from controller gains and low pass filter as shown in Figure 7 which have been tuned by different algorithms like GA, PSO, and MBA. Simultaneous tuning of all the parameters makes the controller faster and more efficient that's why the frequency response of the system is better as the system is associated with 2DOF-PID controllers. 2DOF-PID controller has been used in [34] to control the frequency and tie line power of interconnected system where this controller is shown to be better than traditional PID controller.

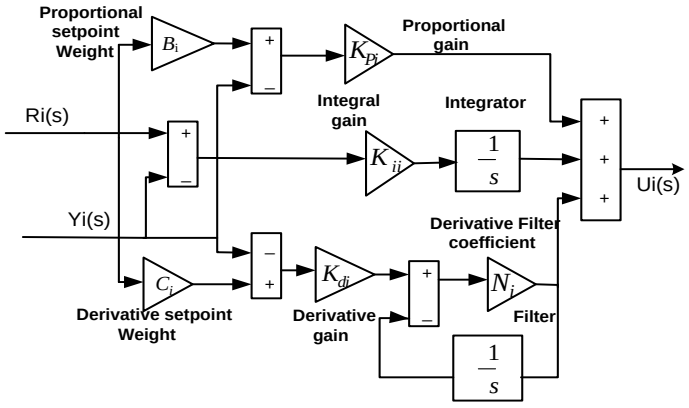

Fig. 7 Simulink model of 2DOF-PID controller

Many papers have used automatic intelligent controllers to contain different parameters as system frequency is contained by PSO based intelligent controllers [31]. On that account, in this study GA and PSO based artificial intelligence are used for the optimization of controller parameters. Moreover, a new

meta-heuristic algorithm (MBA) has been considered for this problem, since papers [32, 33] show the better performance of MBA compared to GA and PSO.

4. Results and Discussions

Dynamic responses of the proposed 3A-HμGS are investigated by using GA, PSO and MBA based methodologies. The system components are modeled with first order linear transfer function considering reasonable approximations. For this study, 0 and 10 are taken as lower and upper limit of controller gain for optimum results. Proposed system has been performed and analyzed under SIMULINK/MATLAB environment for various loading and generating conditions in the next section which are as follows:

Case 1: Dynamic responses of the system parameters when $\Delta v_W = 0, \Delta G = 0, \Delta I = 0, \Delta T = 0$ *and* $\Delta T_a = 0$.

This case study demonstrates and analyzes 3A-HμGS with ±5% load perturbation in each area and no variation in the parameters (i.e. v_W, G, I, and T remain same) of renewable energy sources. Step perturbation in the load is taken at t = 0s and the system performance has been controlled through GA, PSO and MBA based PID, PIDN, and 2DOF-PID controllers. Under this scenario, dynamic responses of area frequencies ΔF_1, ΔF_2, and ΔF_3 have been shown in Figure 8, 9, and 10 respectively. At t = 0s, load is increased by 5% which causes the fall in frequency instantly and after few seconds the frequency deviation is settled down to approximately zero due to proper coordination between sources and storage system through different controlling actions. For quantitative analysis of the proposed hybrid system, important parameters like maximum overshoot (MOS), maximum undershoot (MUS), and settling time (ST) of the frequencies have been summarized in Table-1. With thorough analysis of system responses, it can be observed that MBA based methodology used to tune the controller gains gives better results amongst all of three in terms of MOS, MUS, and ST. Quick settlement in the frequency deviation is achieved through MBA based controllers that's why in the next two cases only MBA based controllers are considered. GA, PSO, and MBA based controllers gains are presented in Table-2, 3, and 4 respectively.

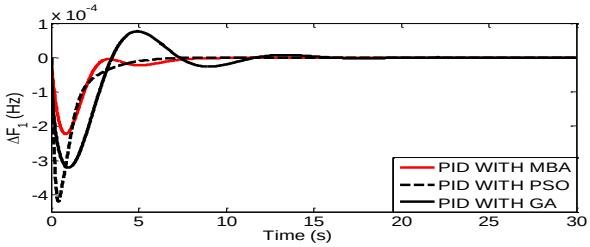

(a)

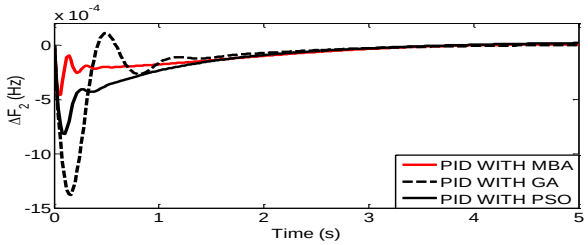

(b)

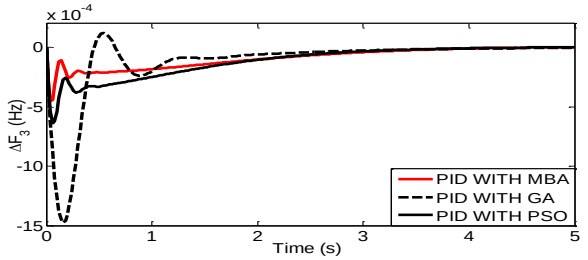

(c)

Fig. 8. Responses of area frequencies controlled by GA, MBA, and PSO based PID controllers

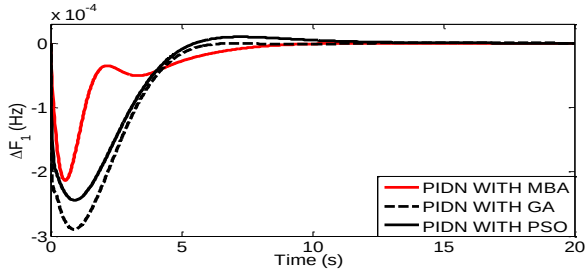

(a)

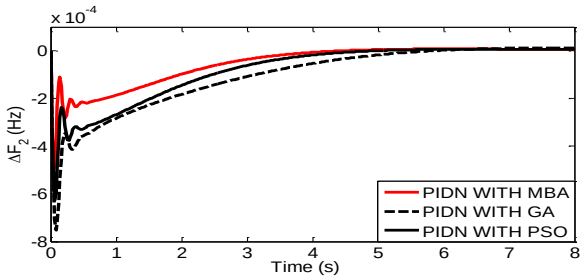

(b)

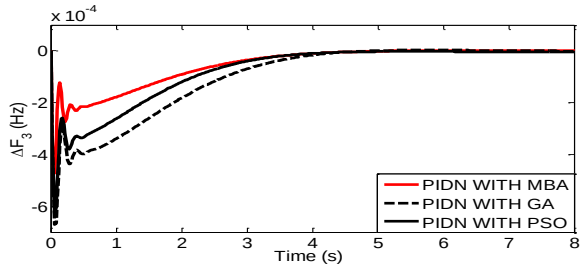

(c)

Fig. 9. Responses of area frequencies controlled by GA, MBA, and PSO based PID controllers with filter.

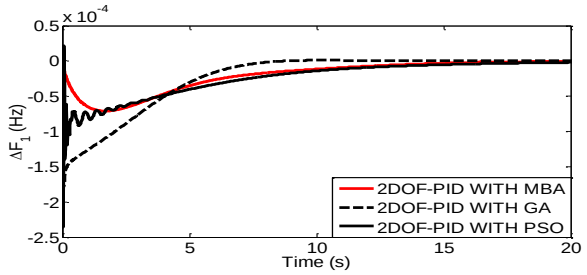

(a)

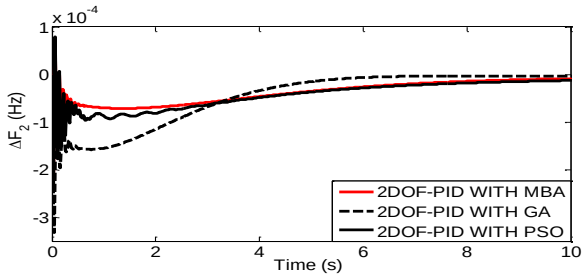

(b)

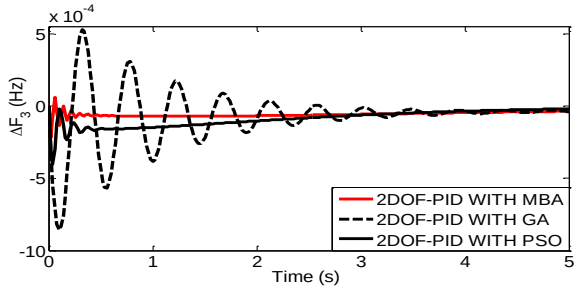

(c)

Fig. 10. Responses of area frequencies controlled by GA, MBA, and PSO based 2DOF-PID controllers.

Case 2: Dynamic responses of the system parameters, when $\Delta v_W = \pm\, 2m/s$, $\Delta G = \pm 0.07\ kW/m^2$, *and* $\Delta I = 0.14\ kW/m^2$ *occur at 25s, 70s, and 110s respectively.*

This case considers wind velocity change of ± 2m/s, and irradiance change for PV arrays and PTC are 70 W/m^2 and 140 W/m^2 respectively in order to incorporate the realistic features of the renewable sources up-to some extent. This change in wind velocity, irradiance change for PV arrays and PTC occur at 25s, 70s, and 110s respectively. Since three renewable sources are associated with three different areas, thus disturbances due to WTG, PTC, and PV arrays actually occur in area 1, area 2, and area 3 at 25s, 70s, and 110s respectively. Moreover, ±5% load perturbation is given in all the three areas at same instant t = 0s.

Pertaining to the mentioned scenario, area frequency deviations ΔF_1, ΔF_2, and $\Delta F_3$are depicted in Figure 11(a)-(c) respectively for different controllers. At 0s, load demand is higher than generation that's why fall in frequency is observed whereas rise in frequency occurs at 25s, 70s, and 110s, because total generation is higher than the load demand due to increase in wind velocity and solar irradiance. Performances of MBA based PID, PIDN and 2DOF-PID controllers are graphically compared. Having compared the frequency responses of the system in terms of MOS, MUS, and ST under different controlling actions, it can be said that the controlling action of 2DOF-PID controller is more effective in minimizing the oscillations. Parameters of controller gains are encapsulated in Table-5.

Table 1: Deviations in area frequencies and oscillation time

	Deviation		*GA*	*PSO*	*MBA*
PID CONTROLLER	F_1	*MOS (in10^{-4})*	-	0.7611	-
		MUS (in10^{-4})	4.1734	3.2109	2.2223
		ST (s)	8.4689	16.483	8.4689
	F_2	*MOS (in10^{-4})*	1.0695	-	-
		MUS (in10^{-4})	13.784	8.2145	4.5633
		ST (s)	3.9615	3.9615	3.9615
	F_3	*MOS (in10^{-4})*	1.0854	-	-
		MUS (in10^{-4})	14.963	6.2154	4.4896
		ST (s)	3.2007	3.2007	3.2007
PIDN CONTROLLER	F_1	*MOS (in10^{-4})*	0.0857	0.8719	-
		MUS (in10^{-4})	2.8921	2.4414	2.1334
		ST (s)	8.6993	12.320	8.6993
	F_2	*MOS (in10^{-4})*	-	-	-
		MUS (in10^{-4})	7.5217	6.2754	4.9435
		ST (s)	6.2203	4.4223	4.4223
	F_3	*MOS (in10^{-4})*	-	-	-
		MUS (in10^{-4})	6.6219	6.2703	4.7211
		ST (s)	4.4281	4.4281	4.4281
2DOF-PID CONTROLLER	F_1	*MOS (in10^{-4})*	-	-	-
		MUS (in10^{-4})	1.7725	2.3546	0.6741
		ST (s)	12.882	16.502	16.368
	F_2	*MOS (in10^{-4})*	-	0.7958	0.6625
		MUS (in10^{-4})	3.3194	2.3041	2.1476
		ST (s)	10.000	10.000	10.000
	F_3	*MOS (in10^{-4})*	5.2007	-	0.6138
		MUS (in10^{-4})	8.5712	4.0325	2.2241
		ST (s)	4.9615	2.7844	0.6214

Table 2: Parameters of PID controller optimized by MBA, PSO and GA

	Gain	MBA	PSO	GA
PID 1	K_{P1}	3.1651	4.1164	2.0118
	K_{I1}	4.9368	1.2826	0.0014
	K_{D1}	4.9443	1.4754	1.8534
PID 2	K_{P2}	4.9496	3.4157	1.9548
	K_{I2}	3.6261	3.9025	4.6020
	K_{D2}	1.2531	0.4170	5.0051
PID 3	K_{P3}	3.2125	4.1176	1.6708
	K_{I3}	4.4539	4.5292	4.0017
	K_{D3}	4.9828	4.4629	5.0185
PID 4	K_{P4}	7.9570	4.7818	4.0271
	K_{I4}	4.5935	3.2638	3.0603
	K_{D4}	4.9200	0.5330	1.7813
PID 5	K_{P5}	2.7014	0.1226	4.4394
	K_{I5}	2.2726	2.5299	1.8510
	K_{D5}	5.0095	2.6927	0.8554
PID 6	K_{P6}	7.9976	4.3219	4.9987
	K_{I6}	4.9802	3.7228	4.1899
	K_{D6}	4.9816	0.4960	3.0736

Table 3: Parameters of PIDN controller optimized by MBA, PSO, and GA

	Gain	MBA	PSO	GA
PIDN 1	K_{P1}	2.6262	4.2410	4.5194
	K_{I1}	8.5345	3.9518	1.6434
	K_{D1}	3.3450	0.8435	0.4480
	N_1	444.85	870.31	649.82
PIDN 2	K_{P2}	6.8462	2.3818	1.0607
	K_{I2}	3.9833	0.0010	2.3155
	K_{D2}	1.9360	5.0000	4.6565
	N_2	434.50	670.77	121.02
PIDN 3	K_{P3}	4.6563	5.0000	1.5584
	K_{I3}	4.5806	1.4392	1.9860
	K_{D3}	3.8040	1.1882	3.9599
	N_3	463.25	707.39	732.57
PIDN 4	K_{P4}	7.9972	5.0000	4.9511
	K_{I4}	3.8070	2.9280	2.1469
	K_{D4}	4.9973	3.4647	2.3048
	N_4	499.93	556.84	699.88
PIDN 5	K_{P5}	8.9929	1.6301	4.5013
	K_{I5}	4.9479	0.0010	0.4908
	K_{D5}	4.9921	1.4387	1.4776
	N_5	497.60	889.40	908.18
PIDN 6	K_{P6}	8.0754	5.0000	3.7309
	K_{I6}	4.9994	3.8876	2.8715
	K_{D6}	4.9991	3.3589	3.1047
	N_6	499.29	708.33	279.59

Table 4: Parameters of 2DOF-PID controller optimized by MBA, PSO and GA

	Gain	MBA	PSO	GA
2D O	K_{P1}	4.9621	4.3039	2.8741
	K_{I1}	8.5812	5.0000	2.8059
	K_{D1}	4.1508	0.0010	1.0987
	N_1	860.65	599.17	234.19
	B_1	4.6018	2.9449	2.5037
	C_1	4.6306	1.1834	0.3489
2D0F-PID 2	K_{P2}	7.3998	3.2952	2.9525
	K_{I2}	2.4623	3.0671	2.7907
	K_{D2}	3.9247	5.0000	4.2520
	N_2	922.15	851.18	1000.0
	B_2	0.6072	5.0000	2.6579
	C_2	3.0364	2.1300	1.0194
2DOF-PID 3	K_{P3}	4.6786	4.5861	3.8311
	K_{I3}	4.9980	5.0000	0.7691
	K_{D3}	4.9835	2.1086	2.5686
	N_3	999.61	788.00	925.53
	B_3	4.6354	3.5313	3.6348
	C_3	2.5745	3.8359	3.5739
2DOF-PID 4	K_{P4}	4.8772	5.0000	1.9590
	K_{I4}	4.4794	5.0000	4.4623
	K_{D4}	4.9992	4.6349	4.7447
	N_4	872.40	598.22	761.30
	B_4	4.6660	4.8133	4.8732
	C_4	4.9784	5.0000	2.6755
2DOF-PID 5	K_{P5}	4.7218	4.2108	0.1019
	K_{I5}	3.2484	0.0015	3.4457
	K_{D5}	4.6843	5.0000	0.1210
	N_5	953.12	1000.0	599.43
	B_5	2.3689	0.2608	3.6197
	C_5	3.8776	3.8773	0.3236
2DOF-PID 6	K_{P6}	4.9979	5.0000	3.8552
	K_{I6}	4.9997	3.9007	4.7620
	K_{D6}	4.5566	0.0010	2.7512
	N_6	501.90	500.00	667.80
	B_6	4.9980	4.1031	2.9427
	C_6	4.9425	0.0940	2.9207

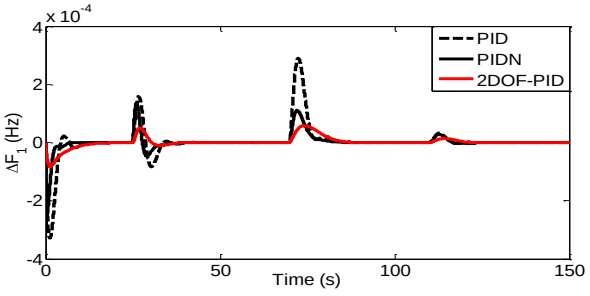

(a)

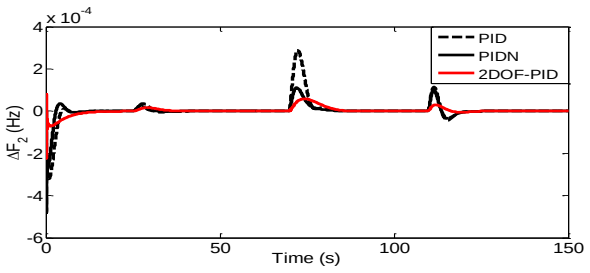

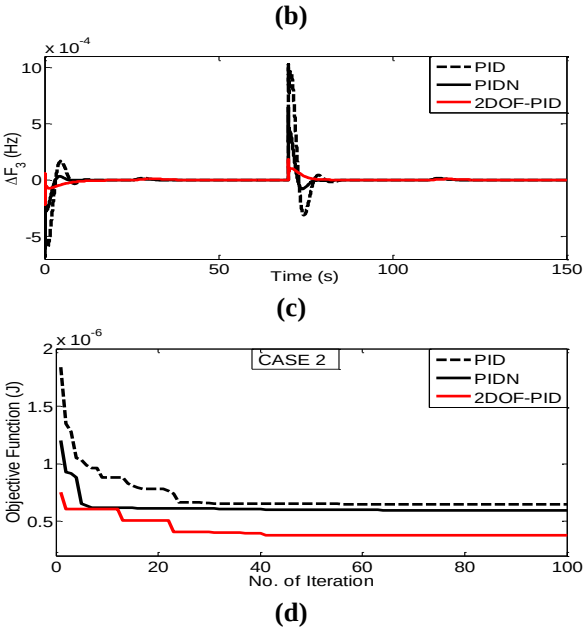

Fig. 11. Dynamic responses of frequencies for (a) area-1 (b) area-2 (c) area-3 when WTG in area-1, PTC in area-2, and PV arrays in area-3 are considered with ± 5% change in load and (d) convergence curve.

Table 5: Parameters of controllers optimized by MBA

	Gain	*PID*	*PIDN*	*2DOF-PID*
PID 1	K_{P1}	0.9660	0.0282	5.2548
	K_{I1}	1.7010	5.0000	4.4766
	K_{D1}	2.9911	0.3071	4.8440
	N_1	-	996.35	490.32
	B_1	-	-	4.6269
	C_1	-	-	4.0089
PID 2	K_{P2}	3.9310	4.1020	3.2522
	K_{I2}	4.5490	4.3247	0.9008
	K_{D2}	4.8023	4.8680	0.7619
	N_2	-	964.26	347.91
	B_2	-	-	4.9056
	C_2	-	-	4.7576
PID 3	K_{P3}	0.9984	4.7572	3.3823
	K_{I3}	1.9285	4.9818	4.9944
	K_{D3}	2.8451	4.6063	4.1294
	N_3	-	983.34	454.64
	B_3	-	-	4.9326
	C_3	-	-	4.8047
PID 4	K_{P4}	4.0000	5.0000	4.9801
	K_{I4}	4.8513	4.9981	4.4640
	K_{D4}	5.0000	5.0000	4.9980
	N_4	-	993.30	499.36
	B_4	-	-	4.9662
	C_4	-	-	4.7487
PID 5	K_{P5}	4.000	5.0000	4.8673
	K_{I5}	5.0000	4.5617	4.9091
	K_{D5}	4.3269	4.7164	4.9249
	N_5	-	908.52	454.57
	B_5	-	-	5.0000
	C_5	-	-	4.5813
PID 6	K_{P6}	0.9927	5.0000	5.0000
	K_{I6}	2.0000	5.0000	5.0000
	K_{D6}	2.6016	5.0000	4.7267
	N_6	-	999.88	484.95
	B_6	-	-	5.0000
	C_6	-	-	4.9979

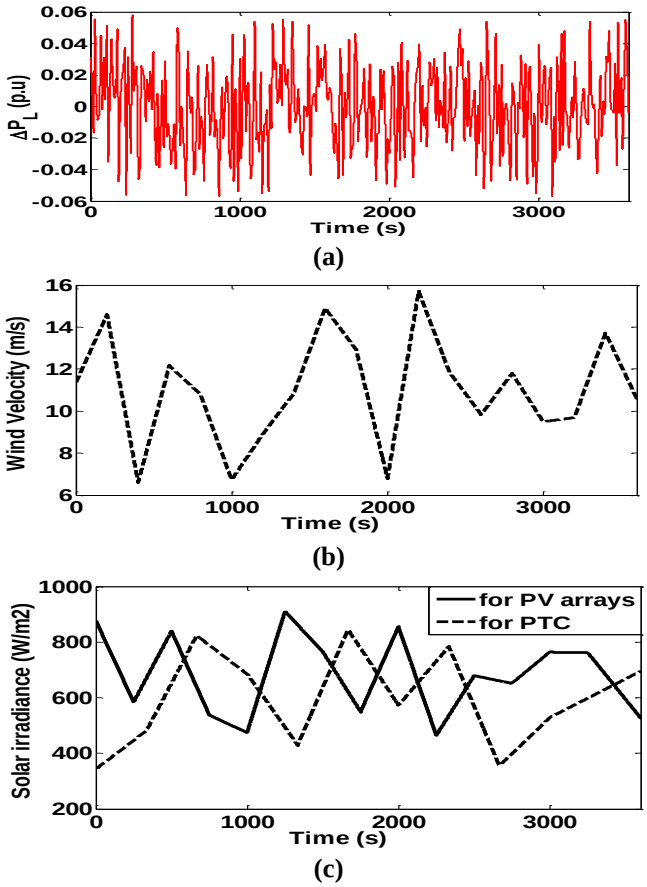

Fig. 12. (a) Variable load (b) varying wind velocity with cut in speed of 6 m/s. (c) direct normal irradiances for PV arrays and PTC.

Case 3: Dynamic responses of the system parameters with different controllers under random variation in load and renewable power generations.

To make 3A-HμGS more realistic a continuous load variation shown in Figure.12 (a) and continuous variation in the parameters of renewable energy sources shown in Figure. 12 (b) and (c) are taken into consideration. Mean variation in the load is about ± 5% in area-1 only for 3600 s (1 Hr.). A change in load and generation is considered for longer duration to observe the practical behavior of the proposed system. Cut-in speed of the wind velocity considered in this case is 6 m/s. A large frequency deviation due to frequent change in power generation and load demand is greatly reduced by coordinated

participation of ESSs with the proposed system. The responses of frequencies are illustrated in Figure. 13 (a)-(c). Once again MBA based 2DOF-PID controller can be easily verified to be better than others in terms of MOS, MUS, and ST of the frequencies. All the Controller gains tuned by MBA are depicted in Table 6.

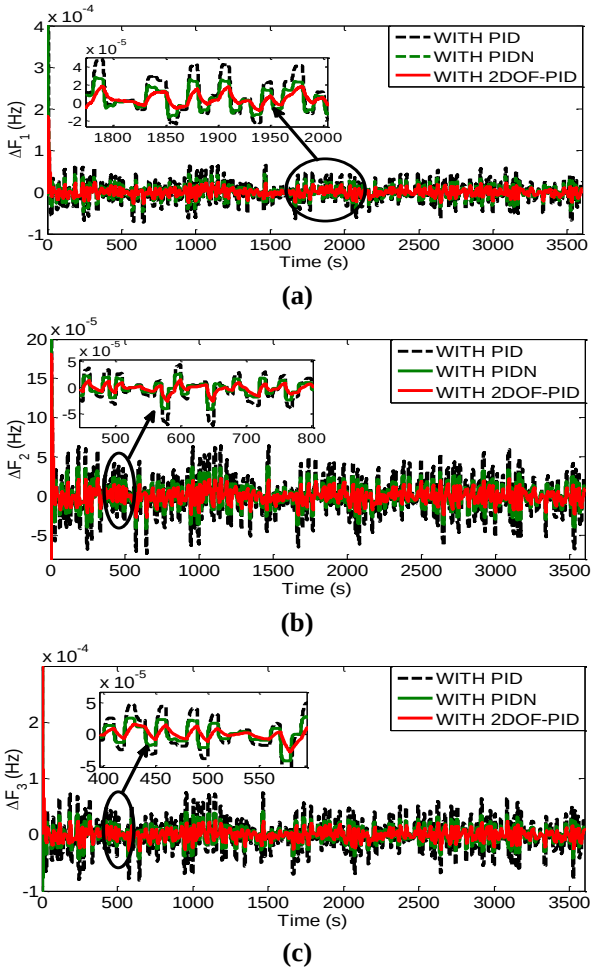

Fig. 13. Dynamic responses of frequencies for (a) area-1 (b) area-2 and (c) area-3 when WTG in area-1, PTC in area-2, and PV arrays in area-3 generate variable powers in association with ESSs and about ± 5% load change in each area.

Table 6: Parameters of controllers optimized by MBA

	Gain	*PID*	*PIDN*	*2DOF-PID*
PID 1	K_{P1}	9.6468	4.9987	1.1648
	K_{I1}	9.8242	4.9804	4.7959
	K_{D1}	9.9785	4.9933	2.0265
	N_1	-	499.66	1000.0
	B_1	-	-	3.7707
	C_1	-	-	0.5677
PID 2	K_{P2}	9.3489	4.9765	4.6477
	K_{I2}	5.7813	4.9971	4.9904
	K_{D2}	9.9858	4.9720	0.0091
	N_2	-	493.65	996.41
	B_2	-	-	3.5220
	C_2	-	-	2.2907
PID 3	K_{P3}	5.5979	4.9854	4.9871
	K_{I3}	9.2957	4.9808	3.9784
	K_{D3}	9.2042	4.6110	4.1083
	N_3	-	498.89	997.16
	B_3	-	-	2.1366
	C_3	-	-	4.7363
PID 4	K_{P4}	9.9505	4.9954	5.0000
	K_{I4}	9.9998	4.9991	4.9231
	K_{D4}	3.5186	4.9980	4.9888
	N_4	-	498.22	916.51
	B_4	-	-	1.3540
	C_4	-	-	2.5416
PID 5	K_{P5}	9.9977	4.9900	4.4747
	K_{I5}	9.9934	4.9970	4.9759
	K_{D5}	8.3128	2.3518	4.9996
	N_5	-	125.13	998.10
	B_5	-	-	4.6600
	C_5	-	-	5.0000
PID 6	K_{P6}	9.9160	4.9990	5.0000
	K_{I6}	10.000	4.9998	5.0000
	K_{D6}	1.1730	1.1606	2.0156
	N_6	-	499.74	699.83
	B_6	-	-	4.7584
	C_6	-	-	2.2633

As detailed in the above mentioned three different cases under various loading and generating conditions, simulations have been carried out to justify the adequacy of the proposed 3A-HμGS. It can be satisfactorily assessed that the frequency deviations found in different cases are within reasonable limits. The simulated results clearly figure out the effectiveness of 2DOF-PID controller in the system to damp out the oscillations.

5. Conclusions

This paper explores the frequency control of 3A-HμGS employed with PID/PID with filter (PIDN)/2DOF-PID controllers. PTC is one of the most promising and sustainable source of energy has been integrated in 3A-HμGS for the first time. Stochastic nature of renewable energy sources particularly, wind and solar cause power and frequency oscillations because of smaller system inertia of the microgrid. Therefore, a controlled coordination between ESSs and RESs is provided through GA, PSO, and MBA based controllers for load frequency control (LFC). Application of PID with filter (PIDN) / 2DOF-PID controllers in such as a 3A-HμGS has not been reported earlier. Having considered the uncertainties in climatic conditions like wind speed variation, temperature change and change in solar irradiances, the simulated results and their analysis clearly signify that the proposed 3A-HμGS and its controlling strategy are appropriate and practically viable. The graphical studies of the system frequencies in all

the cases evidently show that the MBA outperformed the GA and PSO. On comparing the performance of the controllers it has been observed that PIDN controller is better than that of the PID controller, whereas 2DOF-PID controller is better than PIDN controller. However, performance of the MBA based 2DOF-PID controller is the best amongst all other controllers in 3A-HμGS in restricting the frequency oscillations. This work also ensures the practicality of the proposed system as the frequency deviation is controlled within its reasonable limit.

Acknowledgements

We are extremely thankful to NIT Silchar which has supported all the way to execute this study.

References

[1] T. Boukelia, "Parabolic trough solar thermal power plant: potential and projects development in Algeria", Renewable and Sustainable Energy Reviews, pp. 288-297, vol. 21, 2013. (Article)

[2] Solar Thermal Electricity Global Outlook 2016, http://www.solarpaces.org/pressroom/news/item/98-new-solar-thermal-electricity-report. (Standards and Reports)

[3] R. Sebastian, R.P. Alzola, "Simulation of an isolated wind diesel system with battery energy storage", Electr. Power Syst. Res., doi: 10.1016/j.epsr.2010.10.033, pp. 677–686, vol. 81, No. 2, 2011. (Article)

[4] D.C. Das, A.K. Roy, N. Sinha "GA based frequency controller for solar thermal–diesel wind hybrid energy generation/energy storage system", International Journal of Electrical Power and Energy Systems, pp.262-279 vol. 43, 2012. (Article)

[5] A. El-Fergany Attia, A. El-Hameed Mohammed, "Efficient frequency controllers for autonomous two-area hybrid microgrid system using social-spider optimizer", IET Generation, Transmission & Distribution, pp. 637–648 vol. 11, No. 3, 2017. (Article)

[6] M. H. Ali, Wu Bin, and R A. Dougal "An overview of SMES applications in power and energy system", IEEE Transactions on Sustainable Energy, vol. 1, No. 1, 2010. (Article)

[7] Tomonobu Senjyu, Toshiaki Nakaji, Katsumi Uezato, and Toshihisa Funabashi, "A Hybrid Power System Using Alternative Energy Facilities in Isolated Island", IEEE Transactions on Energy Conversion, vol. 20, No. 2, 2005. (Article)

[8] Yong-Song Chen, Sheng-Miao Lin and Boe-Shong Hong: "Experimental Study on a Passive Fuel Cell/Battery Hybrid Power System", Energies, pp. 6413-6422, vol. 6, 2013. (Article)

[9] Omar Hazem Mohammed, Yassine Amirat, Mohamed Benbouzid, Adel Elbast: "Optimal Design of a PV/Fuel Cell Hybrid Power System for the City of Brest in France", IEEE ICGE, pp.119-123, 2014. (Article)

[10] Jae Woong Shim, Youngho Cho, Seog-Joo Kim, Sang Won Min, and Kyeon Hur, "Synergistic Control of SMES and Battery Energy Storage for Enabling Dispatchability of Renewable Energy Sources", IEEE Transactions on Applied Superconductivity, vol. 23 No. 3, 2013. (Article)

[11] S.K. Pandey, S.R. Mohanty, N. Kishor, et al. "Frequency regulation in hybrid power systems using particle swarm optimization and linear matrix inequalities based robust controller design", Int J. Electr. Power Energy Syst., doi: 10.1016/j.ijepes.2014.06.062, pp. 887–900, vol. 63, 2014. (Article)

[12] C.S.A. Nandar, "Robust PI control of smart controllable load frequency for frequency stabilization of microgrid power system", Renew. Energy, doi: 10.1016/j.renene.2012.10.032, pp. 16–23, vol. 56, 2013. (Article)

[13] D. C. Das, A. K. Roy, N. Sinha, "PSO Optimized Frequency Controller for Wind- Solar thermal-Diesel Hybrid Energy Generation System: A Study". International Journal of Wisdom Based Computing, pp. 178-133, vol. 1, No. 3, 2011. (Article)

[14] Datta, Manoj, et al. "A frequency-control approach by photovoltaic generator in a PV–diesel hybrid power system", IEEE Transactions on Energy Conversion, pp. 559-571, vol. 26, No. 2, 2011. (Article)

[15] A. Anil kumar and N. V. Srikanth, "Teaching-Learning Optimization Based Adaptive Fuzzy Logic Controller for Frequency Control in an Autonomous Microgrid", International Journal of Renewable Energy Research, pp. 1842-1849, vol. 7, No. 4, 2017. (Article)

[16] Rabindra Kumar Sahu et al. "Teaching learning based optimization algorithm for automatic generation control of power system using 2-DOF PID controller", International Journal of Electrical Power & Energy System, pp. 287-301, vol. 77, 2016. (Article)

[17] H.M. Hasanien, "A set-membership affine projection algorithm-based adaptive-controlled SMES units for wind farms output power smoothing", IEEE Trans. Sustain. Energy, doi: 10.1109/ TSTE.2014.2340471, pp. 1226–1233, vol. 5, No. 4, 2014. (Article)

[18] WINDPOWERhttp://www.thewindpower.net/turbine_en_42_gamesa_g52-850.php (accessed on 12/Mar/2016). (Standards and Reports)

[19] A. K. Daud, M.S. Ismail, "Design of isolated hybrid systems minimizing costs and pollutant emissions",

Renew. Energy, doi:10.1016/j.renene.2012.01.011, 2012, pp. 215–224, vol. 44, 2012. (Article)

[20] H. Borhanazad, S. Mekhilef, V.G. Ganapathy, et al. "Optimization of micro-grid system using MOPSO', Renew. Energy", doi: 10.1016/j. renene.2014.05.006, pp. 295–306, vol. 71, 2014. (Article)

[21] V. Dudley, et al.: 'Tests results SEGS LS-2 solar collector SAND 94-1884', SANDIA National Laboratories Albuquerque, NM, 1994. (Article)

[22] Al-Nasser, Adel M, "Performance and Economics of a Solar Thermal Power Generation Plant in Jubail, Saudi Arabia: Parabolic Trough Collector", 2010 IEEE International Energy Conference, DOI: 10.1109/ENERGYCON.2010.5771781, pp: 752 – 757. (Conference)

[23] M.J. Montes, A. Abanades, J. M. Martinez-Val, and M. Valdes, "Solar multiple optimization for a solar-only thermal power plant, using oil as a heat transfer fluid in the parabolic trough collectors", science Direct, Solar Energy, 2009, 83(12), pp. 2165-2176. (Article)

[24] L. Wang, D. J. Lee, W. J. Lee et al. "Analysis of a novel autonomous marine hybrid power generation/energy storage system with a high-voltage direct current link", J. Power Sources, doi: 10.1016/j. jpowsour.2008.08.0372008, pp. 1284–1292, vol. 185, No. 2. (Article)

[25] P.K. Ray, S.R. Mohanty, N. Kishor, "Small–signal analysis of autonomous hybrid distributed generation systems in presence of ultra-capacitor and tie–line operation", J. Electr. Eng., doi: 10.2478/ v10187-010-0029-0, pp. 205–214, vol. 61, No. 4, 2010. (Article)

[26] R. Shankar, K. Chatterjee, R. Bhushan, "Impact of energy storage system on load frequency control for diverse sources of interconnected power system in deregulated power environment", Int. J. Electr. Power Energy Syst., doi: 10.1016/j.ijepes.2015.12.029, pp. 11–26, vol. 79, 2016. (Article)

[27] J. Yang, Z. Zeng, Y. Tang, et al. "Load frequency control in isolated micro-grids with electrical vehicles based on multivariable generalized predictive theory", Energies, doi: 10.3390/en8032145, pp. 2145–2164, vol. 8, No. 3, 2015. (Article)

[28] Generation Choices for Microgrids. Available at: http://www.elp.com/articles/print/ volume-93/issue-1/sections/renewables-sustainability/generation-choices-formicrogrids. (June, 2016). (Standards and Reports)

[29] I. Hussain, S. Ranjan, D.C. Das, and N. Sinha, "Performance Analysis of Flower Pollination Algorithm Optimized PID Controller for Wind-PV-SMES-BESS-Diesel Autonomous Hybrid Power System", International Journal of Renewable Energy Research (IJRER), pp.643-651, vol. 7, No. 2, 2017. (Article)

[30] L.I. Zhaosheng, "The optimization design of PID controller parameters based on particle swarm optimization", Fifth Int. Conf. on Advanced Materials and Computer Science (ICAMCS 2016), Qingdao, China, pp. 460–484, 2016. (Conference)

[31] A. Latif, D.C. Das, S. Ranjan, and I. Hussain, "Integrated Demand Side Management and Generation Control for Frequency Control of a Microgrid Using PSO and FA based Controller", International Journal of Renewable Energy Research (IJRER), pp.188-199, vol. 8, No. 1, 2018. (Article)

[32] Ali Sadollah, et al. "Mine blast algorithm: A new population based algorithm for solving constrained engineering optimization problems", Applied Soft Computing, pp. 2592-2612, vol. 13, No. 5, 2013. (Article)

[33] Ali Sadollah, et al. "Mine blast algorithm for optimization of truss structures with discrete variables", Computers & Structures, pp.49-63, vol. 102, 2012. (Article)

Appendix

Specifications and values of different components

WTG- A: 2,124 m^2, start-up v_w: 4 m/s; nominal v_w: 16 m/s; and output voltage: 690 V.

PV arrays - open circuit voltage -36.42 V, short circuit current -8.09 A and maximum operating temperature- 43.2° c.

PTC- Maximum irradiance 1.2 kW/m^2, max fluid temp-700^{0}C.

BESS -150 kWh, Power density 1.2-8 kW/kg.

UC - Capacitance-766.6 F, Equivalent series resistance-3.2mΩ, Power density- 4-10 kW/kg.

SMES - NbTi magnet, system efficiency - 97%, recharging time - <90s.

$K_{WTG} = 1, T_{WTG} = 1.5, K_{PTC} = 1.8, T_{PTC} = 1.8, K_{PV} = 1,$ $T_{PV} = 0.03, T_V = 0.05, K_E = 1, T_E = 0.5, K_P = 1, T_P = 3,$ $T_{12} = T_{23} = T_{13} = 1.4\pi, R_1 = R_2 = R_3 = 0.05,$ B_1=B_2=B_3= 21, K_1= -0.72, K_2= -0.33, K_3= -0.24.